Chapter 9
On-Chip Fabrication, Manipulation and Self-Assembly for Three-Dimensional Cell Structures

Toshio Fukuda, Tao Yue, Masaru Takeuchi and Masahiro Nakajima

Abstract We present an integrated multi-functional microfluidic devices for conducting various tasks, including on-chip fabrication, on-chip manipulation and on-chip self-assembly, for building 3D cellular structures. This system is used for building target cell structures for a "factory line on a chip". This chapter gives a description of the tasks and achievements to show the procedure to our goal, which is focus on the engineered vascular-like cell embedded structures.

Keywords On-chip fabrication · Self-assembly · Photo-crosslinkable resin · Cellular vascular-like microtubes · Microfluidic device · Dielectrophoresis

9.1 Introduction

9.1.1 Motivation in Three-Dimensional Cell Structure for Tissue Engineering

Lost or damage of an organ due to disease or injury is a serious problem for human body. Transplantation of organs to replace the incurable ones is a highly successful therapy [1]. A successful transplant requires a compatible and willing donor. However, the need for donor organs far exceeds the supply [2]. This donor scarcity problem has resulted in new technique which is to build artificial organs by cells and organic materials, which are defined as a tissue engineering [3].

Hence, it will be a great approach to realize artificial organs in vitro environment. Stem cells show promising cell type to achieve the goal. It is required to be grown into a various cell types from the stem cells [4]. Living cells are genetically programmed to assemble themselves into tissues and organs. However, scientists are still in the early stages of understanding how this works [5]. Like in our bodies,

T. Fukuda (✉)
Meijo University, Nagoya University, Beijing Institute of Technology
e-mail: tofukuda@meijo-u.ac.jp

T. Yue · M. Takeuchi · M. Nakajima
Nagoya University

T. Arai et al. (eds.), *Hyper Bio Assembler for 3D Cellular Systems,*
DOI 10.1007/978-4-431-55297-0_9

the tissues and organs are with complex three-dimensional (3D) shapes and structures. Therefore, how to control the positions of cells and form certain shapes by cells as the real tissues are key issues to generate artificial cell tissues [6].

Currently, some researches have been conducted by effective approaches for building two-dimensional (2D) cell structures. The cell growth is controlled on the surface of substrate to form different 2D patterns by changing the surface adhesive properties [7]. Cell positions are controlled and immobilized to 2D shapes via micromanipulation approaches [8]. Arbitrary shaped 2D cell embedded structures are fabricated inside microfluidic devices [9]. Traditionally, many useful and important *in vitro* methods for tissue engineering are contributed by these 2D cell structures. However, numbers of researchers have questions on the validity of studying cells in an environment that is so far away from the *in vivo* state [10]. Tissues and organs are 3D arrangements of cells. 3D shaped structures are necessary for building functional artificial tissues. Besides, in 2D cell structures, the environment is constantly changing while nutrients in the media are depleted and metabolites accumulate. This is clearly different with the *in vivo* state where cells are maintained in a 3D multi-cellular environment of a constant fresh supply of nutrients and the removal of waste products via the circulatory system [11].

Assembly of cells to form 3D shapes and structures offers a practical alternative to natural tissue models. These systems provide an environment in which one or more cell types can be encouraged to form tissues-like constructs. To assemble an artificial organ with working properly, specific cells must be placed in the to specific locations [12]. This is a fundamental issue to be solved for artificial tissue and organ assembly in all living organisms. A specific 3D multi-cellular structure is often critical for proper cellular function. The ability to build such a structure would be useful for the tissue engineering [13]. One useful application would be for organ repair. Another useful purpose would be the study of diseases whose progress is impacted by multi-cellular topology [14].

3D cell models also offer numerous benefits over simple 2D cell models. In recent studies, cell viability, proliferation, differentiation, morphology, gene and protein expression, and function have been shown to exhibit significant differences in 3D compared to 2D, with 3D structures more closely mirroring what is observed *in vivo* [15]. Undoubtedly, 3D cellular structures provide a similar environment for cells as in the real tissues, which enhance the cell proliferation and cell-cell interaction during building artificial tissues. The cell-cell interactions established in 3D play a significant role in the function of both healthy and diseased tissues and can affect the cellular behavior to form tissues. The use of 3D cell structures will add benefits of improved long-term cell viability with a tissue-specific function [16].

9.1.2 Construction Methods for Artificial Tissues

Currently, there are mainly two fundamental construction methods in tissue engineering, which are top-down and bottom-up approaches. The traditional method mentioned in last section belongs to the top-down approaches [17]. In top-down

approaches, cells are seeded on a biodegradable polymeric scaffold and grow according the shape of the scaffold to be a tissue for example. The cells are expected to populate the scaffold and create the appropriate microarchitecture often with the aid of perfusion, growth factors or mechanical stimulations [18]. However, even the surface patterning or more biomimetic scaffolding are used, top-down approaches often have difficulty recreating the intricate microstructural features of tissues [19], because the current biomaterials and micro fabrication methods are with certain limitation for creating intricate 3D biomimetic structures.

On the other hand, bottom-up approaches aim to address the challenge of recreating 3D biomimetic structures by designing structural features on the microscale to build modular tissues that can be used as building blocks to create larger tissues. These modules can be created in many ways, such as through self-assembled aggregation, micro fabrication of cell embedded hydrogels, creation of cell sheets or direct printing of tissues [20, 21]. Once created, these modules can be assembled into larger 3D tissues through a number of methods such as random packing, stacking of cell layers or directed assembly [22–24]. One strong biological basis for this bottom-up approach is that many tissues are also comprised of repeating functional units, such as the lobule in the liver [25]. Consequently, bottom-up approaches are promising to create more biomimetic engineered tissues.

The summary of current construction methods for engineered tissues is shown in Table 9.1. It briefly describes both top-down and bottom-up approaches. In 1997, Dr. Joseph Vacanti grew a human ear from cartilage cells on the back of a mouse, which demonstrated the scaffold based 3D cell structures and tissues [26]. Also,

Table 9.1 Summary of the construction methods for artificial tissues

Approach	Material and method	Advantages	Disadvantages	Refs.
Scaffold	Biodegradable polymer	Directly 3D shape formation	Difficult for complex multi-cellular tissues and cell differentiation	[26–29]
Cell aggregation	Cell beads, cell stimulation	Scaffold-free, multi-cellular structure	Low design flexibility and shape controllability	[30, 31]
Micro fabrication	Hydrogel, photolithography	Arbitrary shape, microscale resolution	Modular tissues need further 3D assembly	[32–35]
Cell sheets and stacking	Cell layers	Scaffold-free, direct transplantation, mass products	Low design flexibility, difficult for complex shapes	[36–38]
Cell printing	Printing, position support	High design flexibility, directly 3D shape formation	Difficult for thick structures, limited resolution	[39–42]
Random assembly	Cell encapsulated units	Microscale resolution, complex structures	Low shape controllability	[24]
Directed assembly	Cell plates	Microscale resolution, self-assembly	Special designed cell plates	[43, 44]

various bottom-up methods are under rapid development. These undergoing issues, such as fabrication of cell blocks, control of cell aggregation and assembly of engineered tissue building blocks, involve manymicrotechnologies including observation, micromanipulation, microfabrication and microfluidic system. Especially, the microfluidic devices integrated with multiple functions provide the promising ways to realize the bottom-up approach (3D cell structure assembly) of tissue engineering.

9.1.3 Research Roadmap of Multi-Functional Microfluidic System

Tissue engineering has great potential to improve the therapy for the tissue and organ damage. It may solve the problem of transplantable organ shortage and suboptimal artificial organs for repair or replacement of diseased or destroyed human organs and tissues. As mentioned above, 3D cell structure assembly will contribute greatly to construct functional tissues. Assembly of cells to form 3D structures provides a biomimetic structures for cells as the real tissue and an environment in which one or more cell types can be encouraged to form tissues-like constructs. Considering the advantages of microtechnologies, the main goal is to integrate these mentioned techniques to develop a 3D cell structure assembly method for constructing artificial tissues inside microfluidic devises. Our research roadmap is depicted in Fig. 9.1, and each part of the system is described as follows.

The first issue is to overcome the limitation of the current available micro tools inside microfluidic devices. We would like to develop the on-chip fabrication and manipulation of arbitrary shaped microstructures to construct functional micro tools directly inside microfluidic devices, in order to build the on-chip cell cultivation for obtaining cell samples with similar characteristics from a single original cell. The

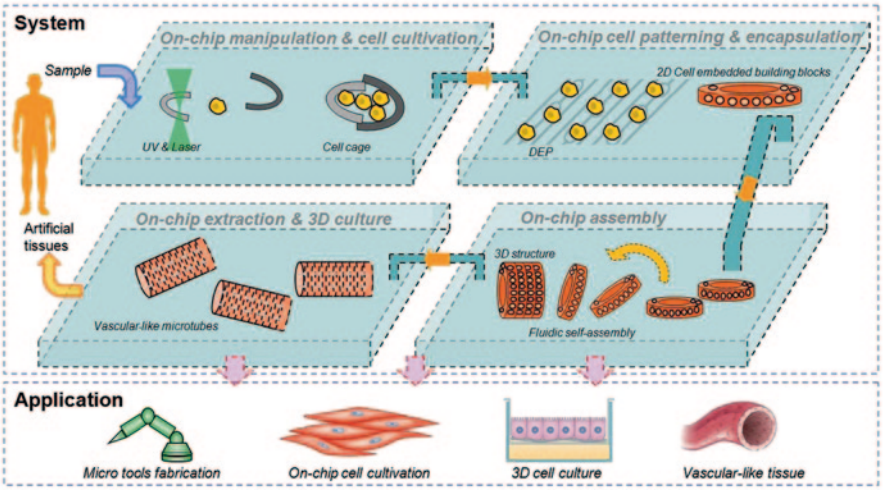

Fig. 9.1 Research roadmap of the whole 3D cell structure assembly inside microfluidic devices

optical microscope, optical tweezers and polydimethylsiloxane (PDMS) microfluidic systems are integrated in one device. Various microstructures can be fabricated and assembled to form micro tools for manipulating cells.

The second issue is to apply the cell samples for the fabrication of 2D micro cell embedded building blocks. We fabricate different shape of micro electrodes and integrate them inside the microfluidic devices. The dielectrophoresis (DEP) will be used to pattern cells. The photo-crosslinkable resin is used to encapsulate patterned cells and fabricate cell embedded components. Different shapes of 2D blocks which are movable and controllable are fabricated directly inside the device, in order to apply in different parts of the artificial tissues.

The third issue is how to make use of the fabricated cell embedded components to construct 3D structures. We develop on-chip assembly method to control the position and attitude of the 2D blocks. Fluidic assembly methods are involved inside multi-functional microfluidic devices. Our objective is to build vascular-like 3D structures based on the previous fabricated components, with high efficiency and contamination-free environment.

Finally, we extract the assembled vascular-like 3D structures outside the assembly channel for their culture. The on-chip extraction function is realized by integrating micro valve system inside the microfluidic devices. The vascular-like shape and multi-cellular condition provide the possible way to generated artificial tissues. We believe our cell assembly method will benefit both the engineering and biological fields.

9.2 On-Chip Fabrication and Manipulation of Arbitrary 2D Cell Embedded Microstructures

9.2.1 On-Chip Fabrication of Arbitrary Microstructures

To assemble 3D cell structures, the fabrication of 2D cell embedded building blocks (microstructures) is the first step. The cells inside real tissues and organs are arranged according to certain patterns and shapes, such as neural cells with line patterns, skin with reticular patterns and blood vessels with tube shapes [45]. To build artificial tissues, an important issue is how to form different patterns of cells as they are really arranged and how to immobilize these patterned cells inside certain structures for encapsulation [46].

For immobilization, the convenient approaches are based on methods such as aspiration, solution pressure and fluidic structure [47]. The advantage of aspiration and pressure is the large fixing force, while the disadvantage is the damage to the cells [48]. Using special fluidic structures, cells are immobilized inside microfluidic devices [49]. On-chip fabrication based on photo-crosslinkable resin via ultra violet (UV) illumination is a creative way of immobilizing cells [50].

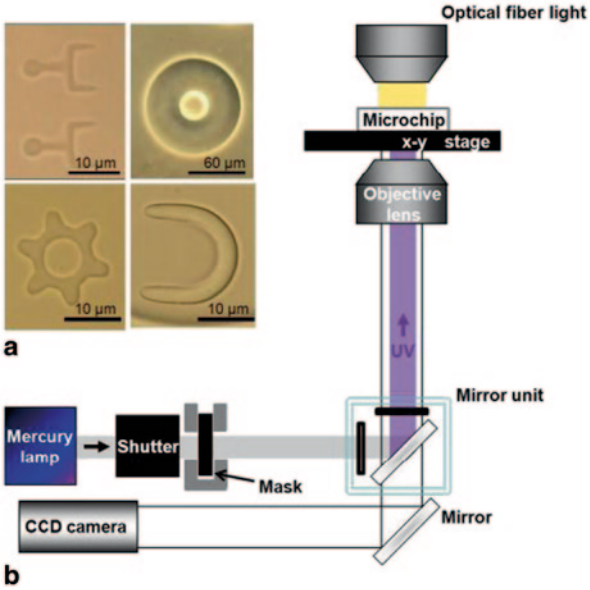

Fig. 9.2 **a** The on-chip fabricated microstructures. **b** The schematic of the on-chip UV fabrication system

We present the on-chip fabrication method for microstructures based on photo-crosslinkable resin [51]. As shown in Fig. 9.2, via the objective lens of a microscope, the patterned UV is illuminated through the mask to the photo-crosslinkable resin, which is inside the microfluidic channel made of PDMS. The microfluidic channel has both glass and PDMS surface for fabricating immovable and movable microstructures respectively. The poly(ethylene glycol) diacrylate (PEGDA) is used as a photo-crosslinkable resin. It is polymerized by the UV light which is patterned for 2D microstructures with arbitrary shapes to fabricate the structures at desired places inside a microfluidic channel [52]. PEGDA has low toxicity and good biocompatibility [53]. Besides, cell viability has been positively confirmed inside PEGDA [54]. It is not needed to prefabricate microstructures or inject the microstructures into the channel from outside. It is possible to fabricate the required microstructures at the desired places. If the cells are mixed inside the photo-crosslinkable solution, they are able to be directly immobilized inside the microstructures by UV exposure.

The fabricated microstructures are shown in Fig. 9.2a. They were fabricated by illuminating the UV-ray for 0.2 s via the objective lens of 100X and 40X. The microstructure fabricated by using 100X objective lens was about 1/100 size compared with the pattern of the mask, while it was about 1/40 size by using 40X lens.

As shown in Fig. 9.2b, the mask made by polyethylene terephthalate (PET) was set in front of the shutter. The patterns on the mask are able to be arbitrary shaped. The UV light was patterned through the mask and exposed into the PEGDA (molecular weight 700) inside the channel of PDMS microfluidic devices. The photo-crosslinkable resin was polymerized and the arbitrary shaped microstructures are fabricated inside the solution.

The position of the microstructure was controlled by the X-Y stage. When the surface of channel bottom is glass, the fabricated microstructure adheres on the glass surface. When the surface of channel bottom is PDMS, the fabricated microstructure is able to move in the non-polymerized resin freely without adhering. Because PDMS has an air permeability and it penetrates oxygen. Oxygen molecule inhibits the radical polymerization of PEGDA. The oxygen layer near the PDMS surface forms a non-polymerized PEGDA layer between the microstructure and PDMS. Thickness of non-polymerized PEGDA layer is about 2 μm. Therefore, the thickness of microstructures depends on the thickness of channel and PDMS surface. For example, inside 40 μm deep channel with both PDMS top and bottom surfaces, the thickness of fabricated microstructure is about 36 μm.

9.2.2 On-Chip Dielectrophoretic Manipulation for Cells Patterning

For manipulation and patterning, existing methods include surface adhesion, optical tweezes and DEP. By using surface adhesion, it is possible to manipulate cells with less causing damage [55]. Optical tweezers is a low-damage cell manipulation system. However, the manipulation force is weak compared with flow resistance [56]. Compared with other methods of cell manipulation, DEP is easier to control and it is non-contact [57]. Due to the low physiological stress caused by DEP, the cells remain viable after treatment and can be cultured for further purposes. By using DEP force, it is possible to manipulate particles with great selectivity. It is also possible to allow the separation of cells or the orientation and manipulation of nanoparticles and nanowires [58]. Furthermore, certain cell sheets with multiple layers are constructed by DEP. Cells aggregate and adhere with each other based on the DEP [59]. Patterned liver cell structures are also formed by DEP traps [60]. Consequently, DEP is widely used for cell manipulation, such as sorting, aggregation and patterning. For immobilization, the on-chip fabrication based on photo-crosslinkable resin via UV illumination is a creative way. Cells are directly immobilized inside the photo-crosslinkable structures. There are several advantages such as high-speed, low-cost and arbitrary shape.

For a spherical particle of radius r suspended in a medium of permittivity ε_m, the DEP force F_{DEP} is given by the expression:

$$F_{DEP} = 2\pi\varepsilon_m r^3 \,\mathrm{Re}[f_{CM}]\cdot\nabla(E_{rms}^2) \tag{9.1}$$

where E_{rms} is a root mean square value of the electric field. $\mathrm{Re}[f_{CM}]$ represents a real part of the f_{CM}, which can be represented as follows:

$$f_{CM} = \frac{\varepsilon_p^* - \varepsilon_m^*}{\varepsilon_p^* + 2\varepsilon_m^*} \tag{9.2}$$

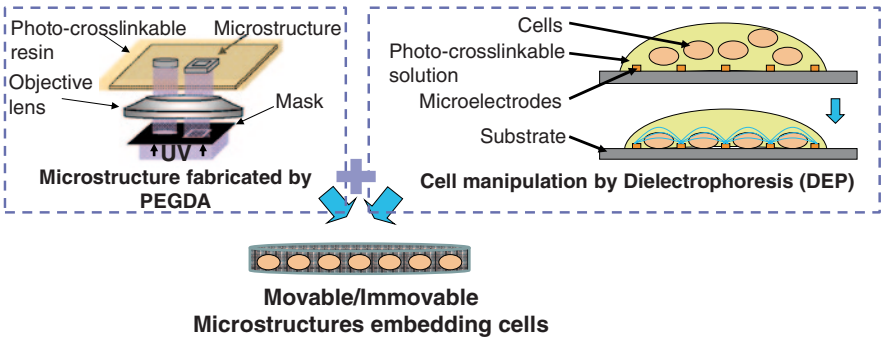

Fig. 9.3 A schematic drawing of the cell assembly method

where ε^* is a complex permittivity which is calculated by $\varepsilon^* = \varepsilon - j\sigma/\omega$, then σ is a conductivity and ω is a frequency of the electric field. Subscripts p and m represent particle and the medium, respectively. Therefore, $\mathrm{Re}[f_{CM}] > 0$ means that the particle shows p-DEP responses so that the particle moves towards the part of the electric field with higher intensity, while $\mathrm{Re}[f_{CM}] < 0$ represents n-DEP response and the particle moves towards the part of the electric field with lower intensity.

We present a method of manipulating particles and cells by DEP and immobilizing them using photo-crosslinkable resin inside microfluidic devices [61]. The whole research approach is shown in Fig. 9.3. The key idea is to create cell structures by combining patterning and immobilizing methods. There are mainly 3 advantages to this approach. First, the non-contact cell patterning method based on DEP is high speed and low-damage. Second, the arbitrarily shaped microstructure is effectively fabricated on-chip inside microfluidic devices. Third, the patterned particles or cells are easily immobilized inside microstructures for further assembly into complex three dimensional (3D) structures.

We developed special microelectrodes of which the size was approximately the same order as the cells. Microelectrodes are key elements in micromanipulation using DEP. Firstly, we used a Indium Tin Oxide (ITO) as a conductive material because it is transparent. The thickness of the ITO layer is 150 nm. The fabrication method was based on photolithography.

The DEP force should be generated inside the solution which means the microfluidic channel is also needed. The PDMS is one of the key components for various microfluidic applications [62]. The mold of the microfluidic channel was made with negative photoresist SU-8. The SU-8 mold was covered with PDMS liquid and cured after 24 h. After the PDMS was detached from the mold, holes were made at the ends of the channel for an inlet and an outlet. The silicone tube was put in the holes then the PDMS was attached on the glass substrate with electrodes. A solution was injected into the channel using negative pressure.

There are two DEP responses of particles: p-DEP and n-DEP. Alternating Current (AC) and NaCl water solutions were used to generate DEP force. By adjusting the frequency of the AC and the concentration of the NaCl solution (medium

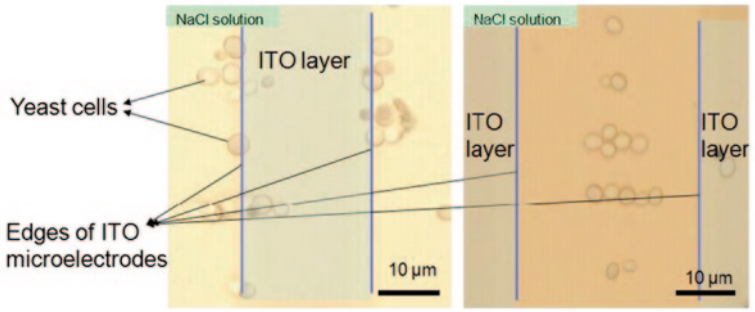

Fig. 9.4 Experiment results of positive dielectrophoresis (p-DEP) and negative dielectrophoresis (n-DEP)

Table 9.2 Different DEP responses under various medium concentrations and the AC frequencies

	100 Hz	1 kHz	30 kHz	500 kHz	1 MHz
90 mg/L	p-DEP	p-DEP	p-DEP	p-DEP	–
200 mg/L	p-DEP	n-DEP	n-DEP	n-DEP	n-DEP
400 mg/L	–	–	–	n-DEP	–

conductivity), these two DEP responses were generated. The reasons for using AC are as follows. First, operating at high frequencies eliminates any electrophoretic movement of the cell. Second, it is possible to eliminate electrochemical reactions at the electrode-electrolyte interfaces, preventing electrode corrosion and gas formation [63].

We confirmed the DEP responses of different particles experimentally such as polymer microspheres, yeast cells (*w303*) as shown in Fig. 9.4. The yeast cells were chosen as microspheres for testing the functions of our system. In order to confirm the precise experimental parameters of p-DEP and n-DEP for yeast cells, the following experimental conditions were used. To generate p-DEP, the concentration of the NaCl solution was 90 mg/L and the frequency of the AC was 1 kHz. To generate n-DEP, the concentration of the NaCl solution was 200 mg/L and the frequency of AC was 500 kHz. In both cases the Vpp of AC was 8 V. Table 9.2 shows the different DEP responses of yeast cells under various medium concentrations and the AC frequencies.

One line of 5 yeast cells was formed. As shown in Fig. 9.5, yeast cells were trapped inside the holes of which the diameter was about 10 μm. It demonstrates the capability of cell traps to manipulate and immobilize the objects in the target position without any contact and damage to the objects.

The n-DEP is often used for manipulating particles. For example, special structures of electrodes are applied to trapping cells at desired positions based on n-DEP [64]. The trapping force is calculated based on the resistance force of the cells given by the liquid flow. After one cell is trapped inside the hole, the flow velocity is

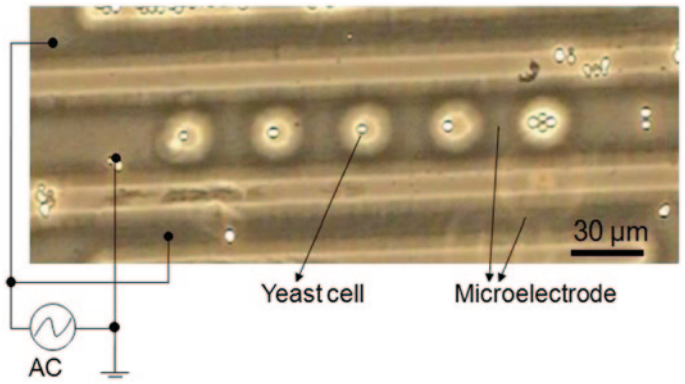

Fig. 9.5 One line of 5 cell traps and trapped yeast cells

increased continually. When the cell escapes from the trap, the trapping force is equal to the resistance force F_r which is calculated by the following expression:

$$F_r = 6\pi\eta v r \tag{9.3}$$

where η is the viscosity of solution, v is the velocity of solution and r is the radius of the cell. The trapping force by DEP in this experiment was about 6 pN.

9.2.3 On-Chip Fabrication of 2D Cell Embedded Microstructures

Based on the on-chip cell patterning method using ITO microelectrodes by DEP forces fabrication method, the fabrication of immovable microstructures embedding patterned yeast cells was conducted.

The experimental steps are follows. First, the ITO microelectrodes and the PDMS microfluidic device were prepared. The ITO microelectrodes were covered with a PDMS mold and formed a microfluidic channel. A solution containing 30% PEGDA (molecular weight 700) and 200 mg/L NaCl was prepared. The PEGDA (700) is able to dissolve in a water. Then the yeast cells (*w303*) were mixed into the solution and the solution was injected into the microfluidic channel. An AC power supply was used to generate DEP force. The frequency of the AC was 500 kHz, and the Vpp of the AC was 8 V. After the cell pattern was formed, the objective lens was adjusted to the patterned position. Then UV light pattern was exposed for 0.2 s to fabricate the microstructures at the same position as the patterned cells. The procedure is schematically shown in Fig. 9.6.

For UV light pattern, donut shaped masks were used. Therefore, after the line patterns of yeast cells were formed, donut-shaped microstructures were fabricated at the same position with UV exposure. This microstructure contains 3 lines of

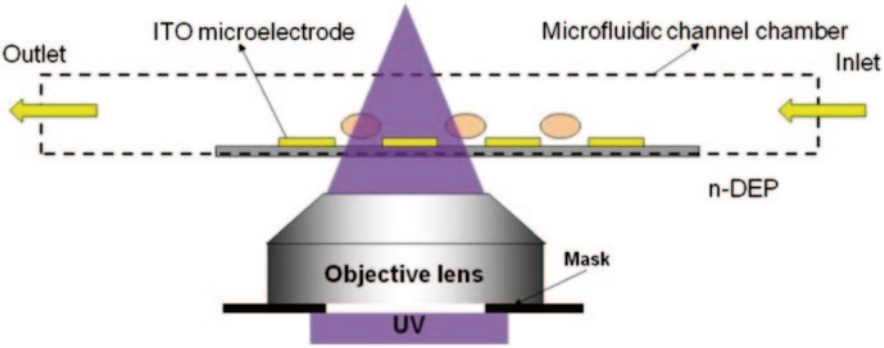

Fig. 9.6 Experimental setup for fabricating microstructures embedding patterned cells

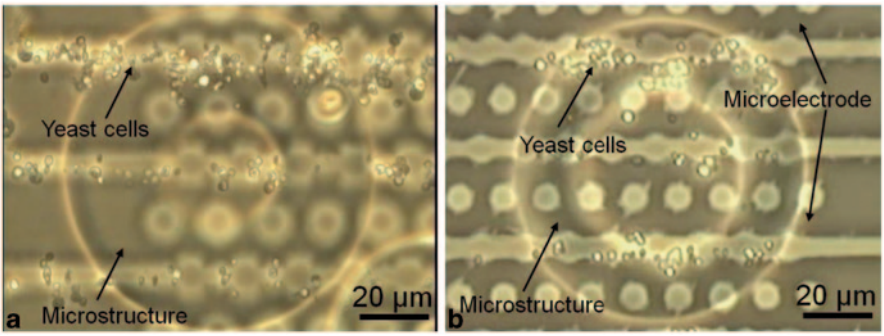

Fig. 9.7 The images of immovable microstructures embedding patterned cells

yeast cells as shown in Fig. 9.7. In Fig. 9.7a, the inner and outer diameter of the donut shapes are 35 and 100 μm respectively. There are approximately 100 yeast cells inside this microstructure. As shown in Fig. 9.7b, after cleaning cells outside the structure by a flowing solution without cells, only the immobilized cells remain clearly inside the microstructure. The pattern was generated in about 10 s and the microstructures were fabricated in 0.2 s. This high speed fabrication is easily controlled and the cells are automatically patterned. Therefore, it is possible to fabricate microstructures very quickly and immobilize large amounts of cells inside them. However, the fabricated microstructures are immovable which means it is difficult to manipulate and assemble them in order to form larger 3D structures.

Figure 9.8 shows the movable microstructures embedding beads or cells. Mammalian cell embedded movable microstructures were fabricated using mouse fibroblast NIH/3T3 cells. After NIH/3T3 cells were cultured inside an incubator, collected cells were mixed with PEGDA solution (30% PEGDAs, 70% Phosphate Buffered Saline (PBS)). Solution was injected inside the microfluidic chip, and then

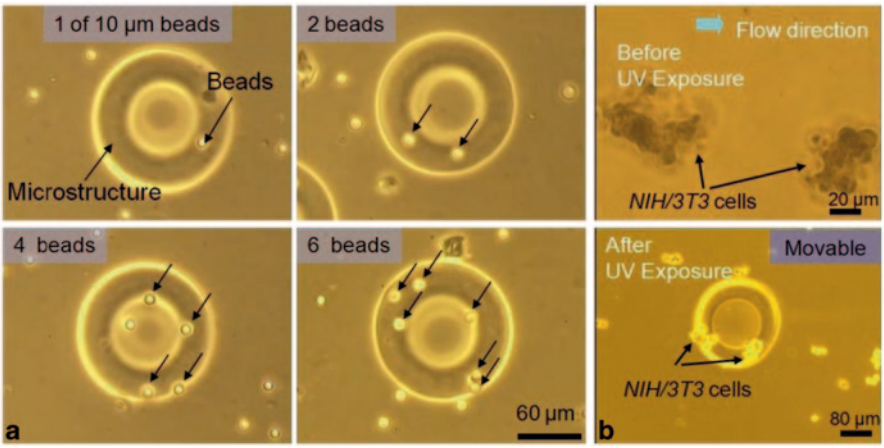

Fig. 9.8 **a** Movable microstructures embedding microbeads of which the concentration or numbers of cells are controllable. **b** Movable microstructures embedding mammalian cells (NIH/3T3)

movable 2D microstructures embedding cells (NIH/3T3) were fabricated directly inside, as shown in Fig. 9.8b.

This high speed fabrication and manipulation shows the great potential of this method for use in high-throughput cell manipulation and immobilization for tissue engineering. These movable microstructures can be further assembled to form much more complex 3D cell structures. With cell culture, these cell embedded microstructures could become functional components of artificial tissues.

9.3 On-Chip Self-Assembly of 2D Microstructures to Multilayered Microtubes

9.3.1 Fluidic Self-Assembly for Multilayered Microtubes

We present a novel method of constructing multi-layered microstructures embedding cells based on on-chip fabrication, micromanipulation system and microfluidic self-assembly inside microfluidic devices [65]. The whole procedure is with high efficiency, high accuracy and control flexibility. The concept of the self-assembly is that, the fabricated microstructures are flowed horizontally with the solution, into the micro well. Following the flow direction, the microstructures are rotated 90 degrees (axis translation from the original position to the assembly position) to be vertical inside the micro well and stopped at the end of the micro well, because they are not able to go into the micro grooves. The stopped microstructures will be assembled one by one. Finally, a tubular 3D structure embedding large amount of cells is formed inside the micro well.

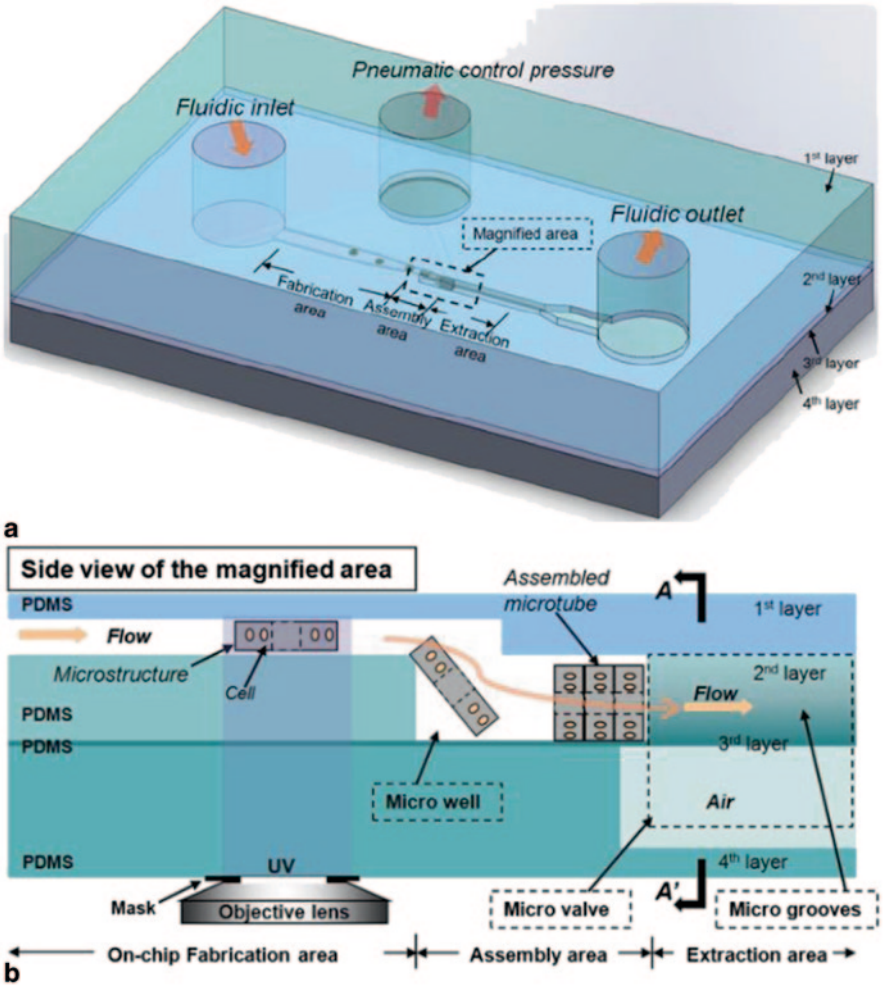

Fig. 9.9 The 4-layer PDMS microfluidic device, with fabrication, assembly and extraction areas. **a** A schematic of whole device. **b** The side view of the magnified area, the fabrication of the microstructures and the self-assembly concept inside the micro well

A microfluidic device with 4 PDMS layers is designed as shown in Fig. 9.9. The 1st layer contains a wide channel for providing a space of microstructure on-chip fabrication, as called the on-chip fabrication area. There is a micro well inside the 2nd layer for assembling the microstructures. There are 3 micro grooves inside the 3rd layer to keep the assembled microstructures in the micro well. The flow can pass through the micro grooves. This part is called the assembly area. There is a channel for acting pneumatic control in the 4th layer by applying negative pressure. The negative pressure can deform the area of micro grooves in the 3rd layer, downwards into the 4th layer. This is called a normally closed (NC) micro valve.

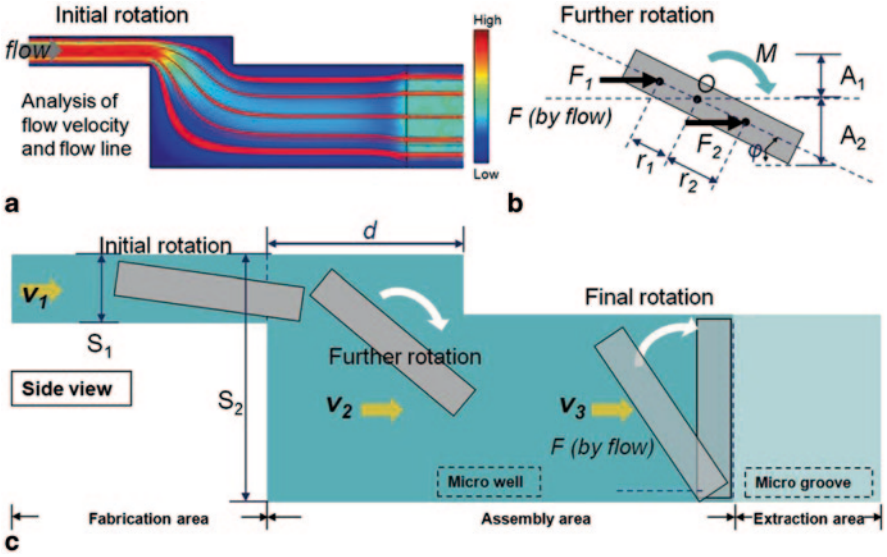

Fig. 9.10 The mechanism of the self-assembly process inside the microfluidic channel

9.3.2 Mechanism of the Self-Assembly Process

The mechanism of the self-assembly process is shown in Fig. 9.10. Its key point is the rotation mechanism of the microstructure. The fabricated microstructure is moved towards the micro well following the flow direction. The flow direction changes when it goes into the micro well as shown in Fig. 9.10a, it causes the initial rotation of the microstructure. The red lines show flow lines and the blue color area represents low flow velocity while the red area represents high. From the simulation result, the velocity difference clearly occurs at the boundary between fabrication area and assembly area. Therefore the microstructure tilts a little as Fig. 9.10b. The average flow velocity in the fabrication area is higher than the assembly area because of the different depth of the channels.

The forces which act on the microstructure in the direction of the fluid flow velocity are important. These forces are called the fluid resistance and expressed as the equation:

$$F = \frac{1}{2} C_d \rho v^2 A \tag{9.4}$$

where C_d is the drag coefficient which related with the shape of the object and the viscosity of the fluid, ρ is the density of the fluid, v is the velocity of the object relative to the fluid, and A is the cross-sectional area of the object. The fluid resistance F_1 (by flow velocity v_1) and F_2 (by flow velocity v_2) act on the different parts of the microstructure (A_1 and A_2 respectively). We also simplify the C_d as the same

for these two forces. These forces generate a torque for rotating the microstructure. The rotation center is shown as point *O*. The torque *M* is calculated as the equation:

$$\begin{aligned} M &= r_1 F_1 \sin\phi - r_2 F_2 \sin\phi \\ &= \frac{1}{2} C_d \rho \sin\phi (v_1^2 r_1 A_1 - v_2^2 r_2 A_2) \end{aligned} \tag{9.5}$$

where *r* is the distance between the point where force *F* is applied and the rotation center *O*, and the length *r* is related with the acting force area *A*. φ is the angle between the microstructure and the horizontal plane. Obviously v_1 is larger than v_2. The r_1 and r_2 have the positive correlation with the A_1 and A_2 respectively. However, with a smaller A_1, the torque may become weaker and it will fail to rotate the microstructure. The A_1 is determined by the Depth of the fabrication channel, and the A_2 is determined by the dimension of the microstructure.

This is the secondary stage of the rotation process for the microstructure, called as a further rotation, shown in Fig. 9.10b. We consider that the further rotation is mainly generated in the place between the fabrication area and the assembly area, which is the distance *d* as shown in Fig. 9.10c. The cross-sectional areas S_1 and S_2 represent the relationship between v_1 and v_2 ($S_1 v_1$ equals $S_2 v_2$) under constant flow rate in the channel. The simplified different flow velocities v_1, v_2 and v_3 in the channel are shown in Fig. 9.10c. The further rotation takes the time *t* and the further rotation angle α can be calculated as:

$$\begin{aligned} \alpha &= \frac{1}{2}\frac{M}{I}t^2 \\ &= \frac{1}{2}\frac{\frac{1}{2}C_d \rho \sin\phi \left(v_1^2 r_1 A_1 - v_2^2 r_2 A_2\right)}{I}\left(\frac{d}{v_2}\right)^2 \\ &= \frac{1}{4}\frac{C_d \rho \sin\phi \left(S_2^2 r_1 A_1 - S_1^2 r_2 A_2\right) d^2}{I S_1^2} \end{aligned} \tag{9.6}$$

where *I* is the rotational inertia of the microstructure. It shows that the flow velocities v_1 and v_2 do not influence the further rotation angle α.

After the further rotation, the micro structure continues to rotate for a while because of the inertia. The microstructure is expected to be rotated less than 90 degrees before the final rotation at the end of the micro well as shown in Fig. 9.10c. With a longer *d*, the further rotation angle will be larger and it may be over 90 degrees. This may cause a failure of the final rotation, especially in the case of 180 degrees. As the rotation dynamic analysis is complicated, the above theoretical analysis is a simplified model for the qualitative analysis. It contributes to the following experiments with different parameters which influence the assembly results.

After a whole successful rotation, the horizontal microstructure becomes vertical and it is assembled at the end of the micro well. As this assembly process is performed by the fluid inside the microchannel, we call it the microfluidic self-assembly.

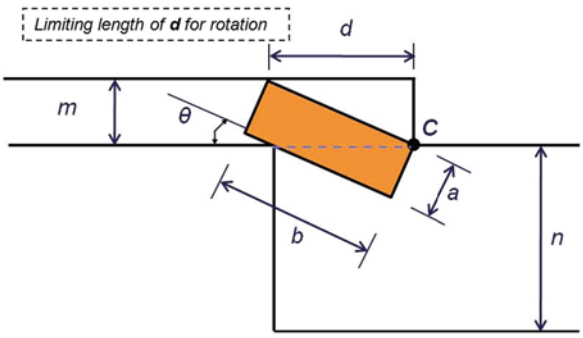

Fig. 9.11 The calculation of the opening length between fabrication area and assembly area, and the minimum length of *d* for microstructures to completely flow into the micro well (*n* is designed according *b*)

In the 2-layer microfluidic channels, a key parameter is the opening length *d* between the fabrication area and the assembly area as shown in Fig. 9.11. The rotation of the microstructures when they flow into the micro well is influenced by the length *d*. There is a minimum length of *d* for the microstructures to completely flow into the micro well. When the corner of microstructure overlaps the corner of channel at the point *C*, and the other corner of microstructure contacts the top of the channel simultaneously, this is a limiting position of the rotation which represents the minimum length of *d*, which is d_{min}. Hence, the d_{min} is calculated by the equation:

$$d_{\min} = ab / m \tag{9.7}$$

The thickness of the microstructure is controlled by the depth of the fabrication channel *m*.

$$a = m - 6 \tag{9.8}$$

It means that the d_{min} is related with the size of microstructure.

A microstructure was fabricated for testing this d_{min}. The 3 types of channels with different opening length *d* were used in the testing experiments. The flow velocity v_2 of these 3 cases was controlled as the same value which was about 25 μm/s. In 120 μm length case which is shorter than minimum length 169 μm, the microstructure did not flow into the micro well. In 170 μm case which is almost the same length as 169 μm, the microstructure flowed into the micro well and rotated about 90 degrees. In 220 μm case which is longer than 169 μm, microstructure rotated more than 90 degrees inside the micro well. A reason of the over rotation is that the *d* is too long. The microstructure rotated too much during going into the micro well. Based on these theoretical calculation and experimental results, the opening length of about 170 μm was characterized as an acceptable parameter for the experimental devices.

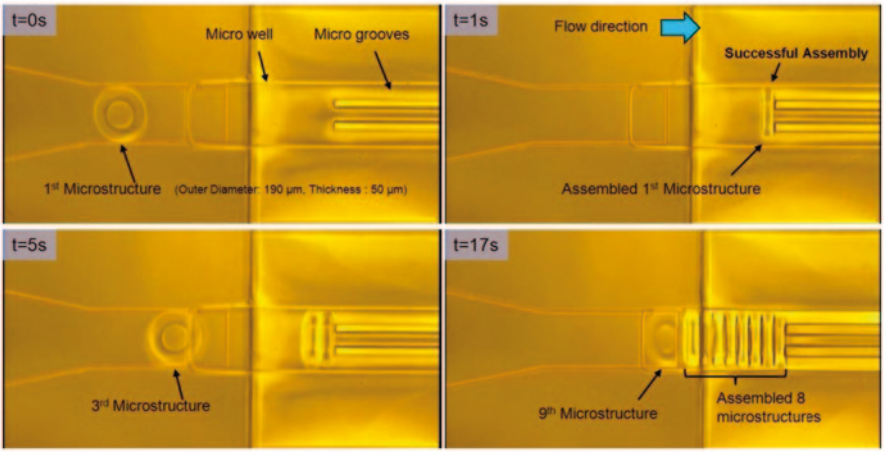

Fig. 9.12 The successful assembly results of 190 μm diameter microstructures with high-efficiency

9.3.3 Evaluation of the Microfluidic Self-Assembly

The on-chip fabrication and microfluidic self-assembly were conducted inside the device. The experimental results of self-assembly are shown in Fig. 9.12. Movable microstructures were continually fabricated inside upper part channel, then they were moved with solution flow into the micro well of bottom part. The inner hollow of this tube-shaped structure is shown clearly in these micrographs. The great advantage of this method is that the whole process is done inside microfluidic channel without any manual manipulation.

Microstructures were continuously fabricated in the fabrication area and then moved with flow into the assembly area. As shown in Fig. 9.12, the fabricated first microstructure successfully went into the micro well and was assembled within 1 s. After 18 s, 9 microstructures were assembled as a tubular structure.

Self-assembly experiments under various flow velocities were conducted to test the effects of the flow velocity. The assembly success rate is defined as the percentage of successful cases in the total assembly cases. By using the microstructures with same size, the velocity difference showed no obvious influence to the assembly success rate. The results are shown in Fig. 9.13a. Considering Eq. (9.6), the experimental results demonstrated that the rotation angle almost did not change under different flow velocities.

Based on Eqs. (9.5) and (9.6), these assembly failures are mainly influenced by the A_1 and A_2, which are the force acting areas related with the dimensions of the microstructure. For the dimensions of microstructures, there are 3 parameters which are the outer diameter (OD.), the inner diameter (ID.) and the thickness. The thickness is controlled by the depth of the fabrication channel which determines the

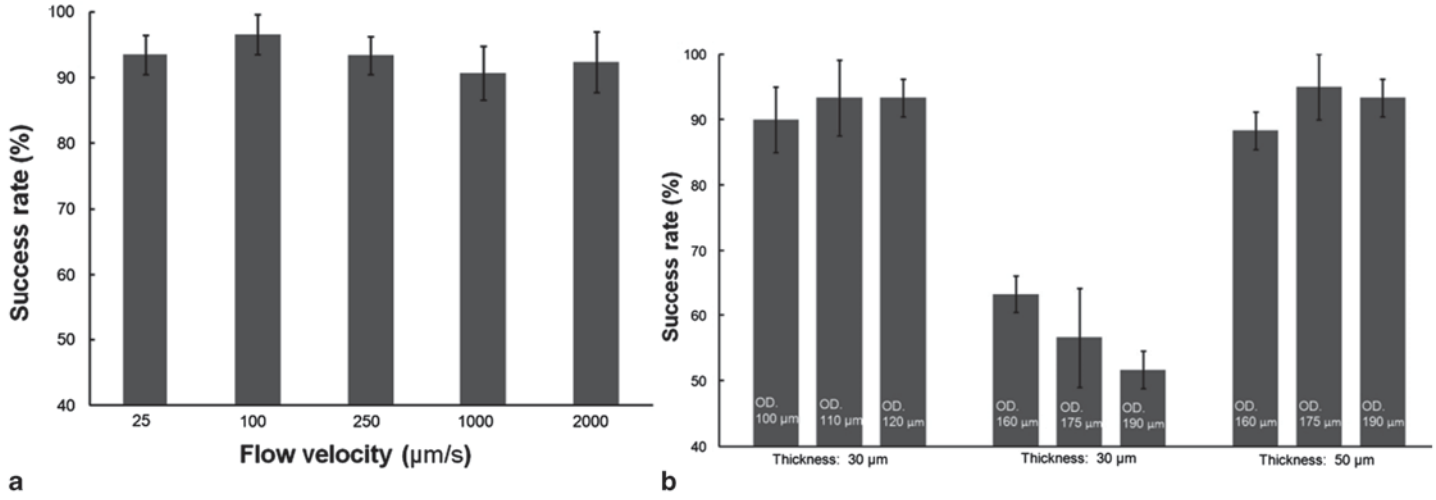

Fig. 9.13 Evaluation results of on-chip self-assembly **a** The evaluation of the relationship between the assembly success rate and the flow velocity. Microstructures with 190 μm in outer diameter were used. The results demonstrated that the rotation angle almost did not change under different flow velocities. **b**The evaluation of the relationship between the assembly success rate and the dimensions of the microstructure. When the ratio of outer diameter to thickness is larger than 5, the success rate decreases tremendously

A_1. The A_2 is mainly influenced by the diameters of the microstructures. However, we design that the inner diameter is always the half size of the outer diameter. It is considered that the outer diameter determines the A_2. Therefore, outer diameter and thickness were evaluated in our experiments.

An evaluation of the relationship between the assembly success rate and the dimensions of the microstructure was conducted as shown in Fig.9.13b. The results are shown in 3groups including 2 different thickness. There were 3 different outer diameters in one group of thickness. All of these cases were conducted under the flow velocity about 250 μm/s. When the thickness was the same, the smaller outer diameter ones showed higher success rate. When the diameter was the same, the larger thickness ones showed higher success rate. The results indicate that when the ratio of outer diameter to thickness is larger than 5, the success rate decreases tremendously.

As shown in Eqs. (9.5) and (9.6), one explanation is that the small thickness represents the small A_1, while the large outer diameter represents the large A_2. It means that the rotation torque M may become smaller and then the rotation of microstructure fails. This evaluation result contributes to determine the better size of microstructures for assembling the microtubes.

9.4 On-Chip Construction of Cellular Vascular-like Microtubes

9.4.1 4-Layer Multi-functional PDMS Microfluidic Device

We demonstrated the on-chip fabrication with extraction of assembled structures from the microfulidic channel. This novel microfluidic device was fabricated with 4 PDMS layers. The fabrication, self-assembly of cell embedded microstructures, and the extraction of assembled tubular structures are all conducted inside this device. It is a reusable microfluidic device and the production of cell embedded microtubes can be conducted continuously.

We proposed microgrooves at NC valve just after the assembly area. This area is named as extraction area, as shown in Fig. 9.14. On-chip extraction was conducted by opening the NC valve. Under the closing condition, it is possible to stop the fabricated microstructures, but release the solution. With the negative pressure, the micro grooves are deformed downwards and the assembled microtube is extracted from the assembly area. The micro valve is commonly used in microfluidic devices for controlling flow [66]. The NC valve is suitable for generating continuously closing of the channel, and also the temporary opening of the channel under the pressure control [67, 68]. Via the opening of the NC valve, the assembled vascular-like microtubes are able to be extracted from the device and transported to the culture

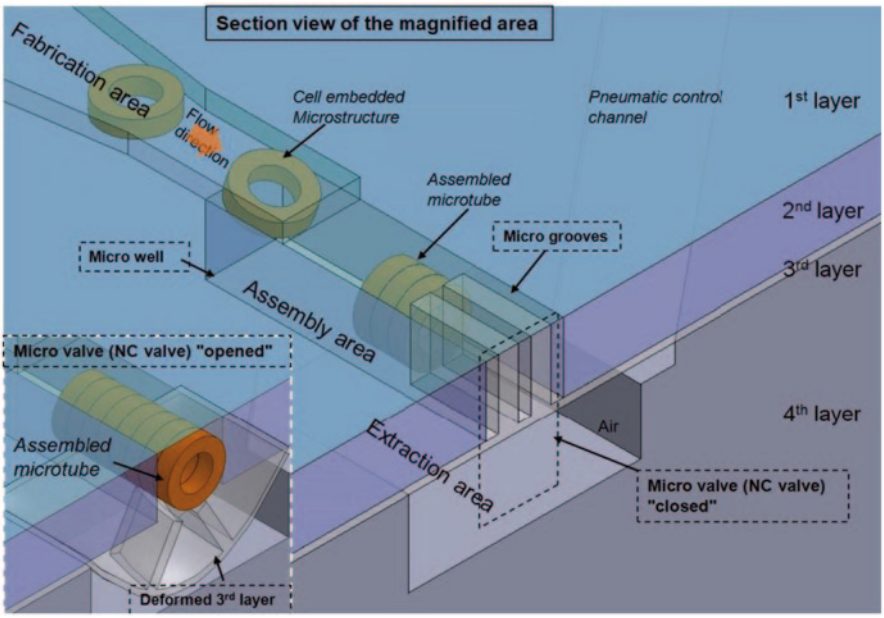

Fig. 9.14 Section view of the magnified area cut at A-A'. When the NC valve is closed without the negative pressure in 4th layer, the self-assembly was conducted in this status. When the NC valve is opened with the negative pressure in 4th layer, the extraction of the assembled microtube was conducted in this status

dishes for further treatments and applications. After extracting this microtube via the micro valve, the negative pressure is tuned off to close the valve, and the new microstructures are able to be fabricated and assembled to construct a new microtube structures.

The on-chip extraction for the microtube was conducted, as shown in Fig. 9.15a. The microtube was stopped by the micro grooves. Then the negative pressure was applied through the pneumatic control channel in the 4th layer to the NC valve area. The micro grooves above the pneumatic control channel of 3rd layer were deformed downwards. After the vertical deformation of 3rd layer was larger than 240 μm, the 3rd layer contacted with 4th layer. By enhancing the negative pressure, the elliptic contact area expanded. The length of the major axis of the elliptic contact area was called the valve opening length. When the valve opening length was longer than the length of the micro grooves, the micro grooves were fully sank in the 4th layer and the valve was fully opened for extracting the microtube. The extraction took about 40 s and the whole microtube was successfully extracted. Figure 9.15b shows the relationship between the applied negative pressure and the valve opening percentage. As the length of micro grooves is 1200 μm, the valve opening percentage is

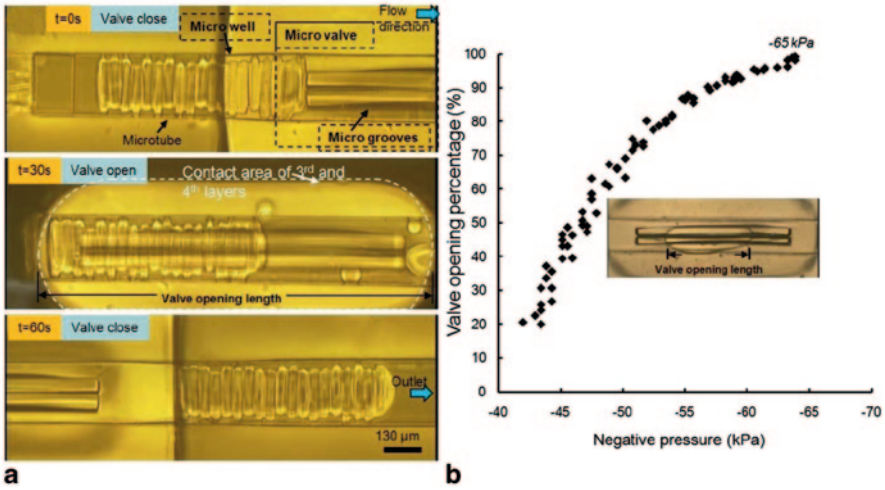

Fig. 9.15 **a** The NC valve was closed for assembly and opened for extraction of the assembled microtube. **b** The relationship between the applied negative pressure and the valve opening percentage. When the negative pressure was lower than −65 kPa, the NC valve was able to be fully opened

defined as the percentage of the valve opening length on 1200 μm. For this device, the negative pressure 65 kPa is needed for fully opening the NC valve and conducting the extraction process.

9.4.2 Assembly of Cell Embedded Microstructures to Microtubes

In order to confirm that the presented method was able to be used in biological applications, cell viability tests were conducted after embedding cells inside the donut-shaped microstructures. The cell embedded microstructures using NIH/3T3 cells were washed by Phosphate Buffered Saline (PBS) then they were immersed in the viability test solution which was the mixture of 10 μL Calcein AM (1 mg/mL), 15 μL Propidium iodide (PI, 1 mg/mL) and 5 mL PBS. The test solution with the microstructures was put inside an incubator (37 °C, 5 % CO_2) for 30 min. After that, the test solution was removed and the microstructures were washed by PBS again. The fluorescent images of the testing results are shown as Fig. 9.16a. The green represents the live cells while the red means the dead cells. Different dimensions of donut-shaped microstructures were used. Figure 9.16b shows that the relative cell viability of all the samples is higher than 80 %, which confirms that they are to be used in biological applications.

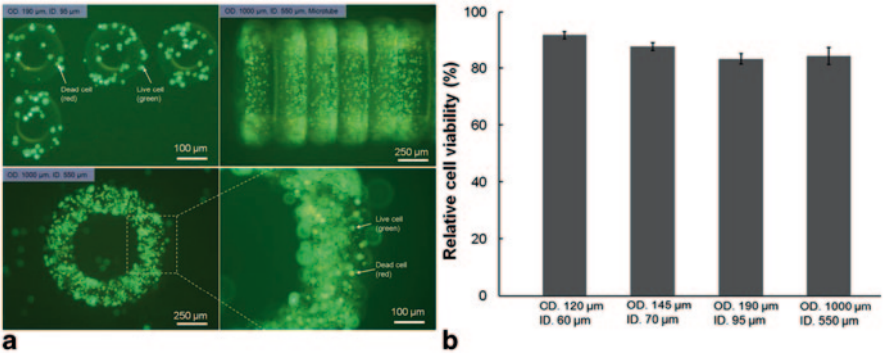

Fig. 9.16 The viability tests for the cells embedded inside microstructures. **a** The green represents the live cells while the red means the dead ones. **b**The relative cell viability of the cells embedded inside microstructures

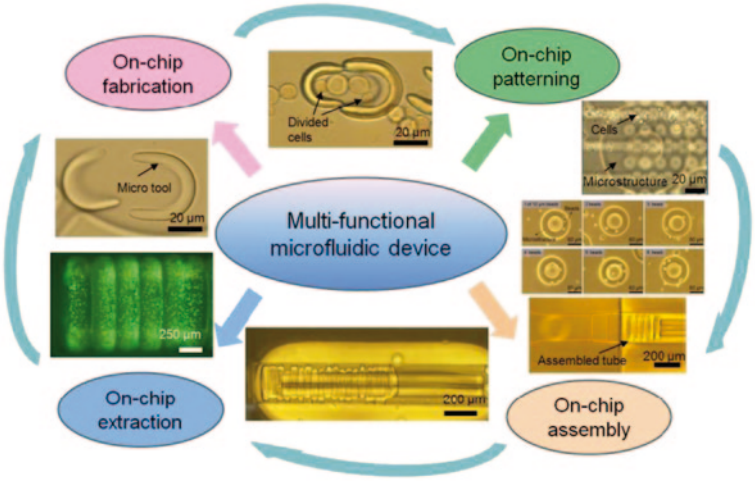

Fig. 9.17 The integrated multi-functional microfluidic system, with the on-chip fabrication, on-chip patterning, on-chip extraction and on-chip assembly

9.5 Conclusion

In this chapter, we focused on building 3D cell structures inside multifunctional microfluidic devices based on a bottom-up method, as shown in Fig. 9.17. It is used as a "factory line on a chip", including on-chip fabrication, on-chip patterning, on-chip assembly and on-chip extraction.

A novel 4-layer PDMS microfluidic device is fabricated, including fabrication area, self-assembly area and extraction area inside one channel. The on-chip fabrication and assembly of microstructures based on photo-crosslinkable resin is

presented. The movable microstructures embedding patterned particles and cells are fabricated inside the microfluidic channel, as the 2D blocks for building 3D structures. The novel fluidic self-assembly of 2D microstructures based on axis-translation process is presented and experimentally demonstrated. The NIH/3T3 cells embedded microtubes are self-assembled and directly extracted outside the channel by the NC micro valve system. The 3D vascular-like microtubes are constructed by our system, with high efficiency and a contamination-free environment. This technology will contribute the construction of functional 3D cell tissues.

The fabricated structures will contribute the construction of functional 3D tissues.

References

1. Langer R, Vacanti JP (1993) Tissue engineering. Science 260:920–926
2. Stock UA, Vacanti JP (2001) Tissue engineering: current state and prospects. Annu Rev Med 52:443–451
3. Vacanti CA (2006) The history of tissue engineering. J Cell Mol Med 10:569–576
4. Emmert MY, Wolint P, Wickboldt N, Gemayel G, Weber B, Brokopp CE, Boni A, Falk V, Bosman A, Jaconi ME, Hoerstrup SP (2013) Human stem cell-based three-dimensional microtissues for advanced cardiac cell therapie. Biomaterials 34:6339–6354
5. Karamichos D, Rich CB, Hutcheon AEK, Ren R, Saitta B, Trinkaus-Randall V, Zieske JD (2011) Self-Assembled matrix by umbilical cord stem cells. J Funct Biomater 2:213–229
6. Mironov V, Boland T, Trusk T, Forgacs G, Markwald RR (2003) Organ printing: computer-aided jet-based 3D tissue engineering. Trends Biotechnol 21:157–161
7. Ishizaki T, Saito N, Takai O (2010) Correlation of cell adhesive behaviors on superhydrophobic, superhydrophilic, and micropatterned superhydrophobic/superhydrophilic surfaces to their surface chemistry. Langmuir 26:8147–8154
8. Lewpiriyawong N, Yang C, Lam YC (2008) Dielectrophoretic manipulation of particles in a modified microfluidic H filter with multi-insulating blocks. Biomicrofluid 2
9. Dendukuri D, Pregibon DC, Collins J, Hatton TA, Doyle PS (2006) Continuous-flow lithography for high-throughput microparticle synthesis. Nat Mater 5:365–369
10. Elliott NT, Yuan F (2011) A review of three-dimensional in vitro tissue models for drug discovery and transport studies. J Pharm Sci 100:59–74
11. Pampaloni F, Reynaud EG, Stelzer EHK (2007) The third dimension bridges the gap between cell culture and live tissue. Nature Rev Mol Cell Biol 8:839–845
12. Mazzoleni G, Lorenzo D, Steimberg N (2009) Modelling tissues in 3D: the next future of pharmaco-toxicology and food research? Genes Nutr 4:13–22
13. Gartner ZJ, Bertozzi CR (2009) Programmed assembly of 3-dimensional microtissues with defined cellular connectivity. Proc Natl Acad Sci 106:4606–4610
14. Huh D, Hamilton GA, Ingber DE (2011) From 3D cell culture to organs-on-chips. Trends Cell Biol 21:745–754
15. Derda R, Laromaine A, Mammoto A, Tang SKY, Mammoto T, Ingber DE, Whitesides GM (2009) Paper-supported 3D cell culture for tissue-based bioassays. Proc Natl Acad Sci 106:18457–18462
16. Moon S, Hasan SK, Song YS, Xu F, Keles HO, Manzur F, Mikkilineni S, Hong JW, Nagatomi J, Haeggstrom E, Khademhosseini A, Demirci U (2010) Layer by layer three-dimensional tissue epitaxy by cell-laden hydrogel droplets. Tissue Eng Part C-Methods 16:157–166
17. Nichol JW, Khademhosseini A (2009) Modular tissue engineering: engineering biological tissues from the bottom up. Soft Matter 5:1312–1319

18. Niklason LE, Gao J, Abbott WM, Hirschi KK, Houser S, Marini R, Langer R (1999) Functional arteries grown in vitro. Science 284:489–493
19. Hahn MS, Miller JS, West JL (2006) Three-dimensional biochemical and biomechanical patterning of hydrogels for guiding cell behavior. Adv Mater 18:2679–2684
20. L'Heureux N, Paquet S, Labbe R, Germain L, Auger FA (1998) A completely biological tissue-engineered human blood vessel. Faseb J 12:47–56
21. Yeh J, Ling Y, Karp JM, Gantz J, Chandawarkar A, Eng G, Blumling III, J, Langer R, Khademhosseini A (2006) Micromolding of shape-controlled, harvestable cell-laden hydrogels. Biomaterials 27:5391–5398
22. Koh WG, Pishko MV (2006) Fabrication of cell-containing hydrogel microstructures inside microfluidic devices that can be used as cell-based biosensors. Anal Bioanal Chem 385:1389–1397
23. L'Heureux N, McAllister TN, de la Fuente LM (2007) Tissue-engineered blood vessel for adult arterial revascularization. New Engl J Med 357:1451–1453
24. Du Y, Lo E, Ali S, Khademhosseini A (2008) Directed assembly of cell-laden microgels for fabrication of 3D tissue constructs. Proc Natl Acad Sci 105:9522–9527
25. Liu Tsang V, Chen AA, Cho LM, Jadin KD, Sah RL, DeLong S, West JL, Bhatia SN (2007) Fabrication of 3D hepatic tissues by additive photopatterning of cellular hydrogels. FASEB J 21:790–801
26. Cao YL, Vacanti JP, Paige KT, Upton J, Vacanti CA (1997) Transplantation of chondrocytes utilizing a polymer-cell construct to produce tissue-engineered cartilage in the shape of a human ear. Plast Reconstr Surg 100:297–302
27. Roh JD, Sawh-Martinez R, Brennan MP, Jay SM, Devine L, Rao DA, Yi T, Mirensky TL, Nalbandian A, Udelsman B, Hibino N, Shinoka T, Saltzman WM, Snyder E, Kyriakides TR, Pober JS, Breuer CK (2010) Tissue-engineered vascular grafts transform into mature blood vessels via an inflammation-mediated process of vascular remodeling. Proc Natl Acad Sci 107:4669–4674
28. Krawiec JT, Vorp DA (2012) Adult stem cell-based tissue engineered blood vessels: a review. Biomaterials 33:3388–3400
29. Bomhard AV, Veit J, Bermueller C, Rotter N, Staudenmaier R, Storck K, The HN (2013) Prefabrication of 3D cartilage contructs: towards a tissue engineered auricle—a model tested in Rabbits. Plos One 8:e71667
30. Matsunaga YT, Morimoto Y, Takeuchi S (2011) Molding cell beads for rapid construction of macroscopic 3D tissue architecture. Adv Mater 23:H90–H94
31. Sakar MS, Neal D, Boudou T, Borochin MA, Li Y, Weiss R, Kamm RD, Chen, Asada, H (2012) H.: Formation and optogenetic control of engineered 3D skeletal muscle bioactuators. Lab Chip 12:4976–4985
32. Chung SE, Park W, Shin S, Lee SA, Kwon S (2008) Guided and fluidic self-assembly of microstructures using railed microfluidic channels. Nat Mater 7:581–587
33. Xu F, Finley TD, Turkaydin M, Sung Y, Gurkan UA, Yavuz AS, Guldiken RO, Demirci U (2011) The assembly of cell-encapsulating microscale hydrogels using acoustic waves. Biomaterials 32:7847–7855
34. Billiet T, Vandenhaute M, Schelfhout J, Van Vlierberghe S, Dubruel P (2012) A review of trends and limitations in hydrogel-rapid prototyping for tissue engineering. Biomaterials 33:6020–6041
35. Lu T, Li Y, Chen T (2013) Techniques for fabrication and construction of three-dimensional scaffolds for tissue engineering. Intl J Nanomed 8:337–350
36. Yamato M, Okano T (2004) Cell sheet engineering. Mater Today 7:42–47
37. Yang J, Yamato M, Kohno C, Nishimoto A, Sekine H, Fukai F, Okano T (2005) Cell sheet engineering: Recreating tissues without biodegradable scaffolds. Biomaterials 26:6415–6422
38. Ohashi K, Yokoyama T, Yamato M, Kuge H, Kanehiro H, Tsutsumi M, Amanuma T, Iwata H, Yang J, Okano T, Nakajima Y (2007) Engineering functional two- and three-dimensional liver systems in vivo using hepatic tissue sheets. Nat Med 13:880–885

39. Jakab K, Norotte C, Marga F, Murphy K, Vunjak-Novakovic G, Forgacs G (2010) Tissue engineering by self-assembly and bio-printing of living cells. Biofabrication 2(2):022001
40. Shimoto T, Nakayama K, Matsuda S, Iwamoto Y (2012) Building of HD MACs using cell processing robot for cartilage regeneration. J Robot Mechatron 24:347–353
41. Forgacs G, Sun W (2013) Biofabrication: micro-and nano-fabrication, printing, patterning and assemblies. Elsevier Inc.
42. Shimoto T, Hidaka N, Sasaki H, Nakayama K, Akieda S, Matsuda S, Miura H, Iwamoto Y (2013) Bio rapid prototyping project: development of spheroid formation system for regenerative medicine. Information Technology Convergence, vol 253. Information Technology Convergence, Springer Netherlands, pp 855–862
43. Kuribayashi-Shigetomi K, Onoe H, Takeuchi S (2012) Cell origami: self-folding of three-dimensional cell-laden microstructures driven by cell traction force. Plos One 7(12):e51085
44. Kato-Negishi M, Morimoto Y, Onoe H, Takeuchi S (2013) Millimeter-sized neural building blocks for 3D heterogeneous neural network assembly. Adv Health Mater 2:1564–1570
45. Suuronen EJ, Sheardown H, Newman KD, McLaughlin CR, Griffith M (2005) Building in vitro models of organs. Intl Rev Cytol 244:137–173. (Kwang WJ ed, Academic Press)
46. Khetani SR, Bhatia SN (2006) Engineering tissues for in vitro applications. Curr Opin Biotech 17:524–531
47. Tsutsui H, Yu E, Marquina S, Valamehr B, Wong I, Wu H, Ho CM (2010) Efficient dielectrophoretic patterning of embryonic stem cells. Ann Biomed Eng 38:3777–3788
48. Tixier-Mita A, Jun J, Ostrovidov S, Chiral M, Frenea M, Le Pioufle B, Fujita H (2004) A silicon micro-system for parallel gene transfection into arrayed cells. Proc. of 8th Intl. Conf. Miniaturized System for Chem. and Life Sciences (uTAS 2004), pp 180–182
49. Di Carlo D, Aghdam N, Lee LP (2006) Single-cell enzyme concentrations, kinetics, and inhibition analysis using high-density hydrodynamic cell isolation arrays. Anal Chem 78:4925–4930
50. Maruyama H, Arai F, Fukuda T (2007) Gel-tool sensor positioned by optical tweezers for local pH measurement in a microchip. Proc. of 2007 IEEE Intl. Conf. Robot. Autom., (ICRA 2007) pp 806–811
51. Yue T, Nakajima M, Takeuchi M, Fukuda T (2014) Improved laser manipulation for on-chip fabricated microstructures based on solution replacement and its application in single cell analysis. Int J Adv Robot Syst 11:11
52. Ito M, Nakajima M, Maruyama H, Fukuda T (2009) On-chip fabrication and assembly of rotational microstructures. Proc. of 2009 IEEE/RSJ Intl. Conf. Intell. Robot. Syst., (IROS 2009) pp 1849–1854
53. Panda P, Ali S, Lo E, Chung BG, Hatton TA, Khademhosseini A, Doyle PS (2008) Stop-flow lithography to generate cell-laden microgel particles. Lab Chip 8:1056–1061
54. Chan V, Zorlutuna P, Jeong JH, Kong H, Bashir R (2010) Three-dimensional photopatterning of hydrogels using stereolithography for long-term cell encapsulation. Lab Chip 10:2062–2070
55. Bernstein RW, Scott M, Solgaard O (2004) BioMEMS for high-throughput handling and microinjection of embryos. Mems/Moems Technol Appl 5641:67–73. Ma Z et al., eds, Bellingham: Spie-Int Soc Optical Engineering
56. Hu S, Sun D (2011) Automatic transportation of biological cells with a robot-tweezer manipulation system. Int J Rob Res 30:1681–1694
57. Jaeger MS, Uhlig K, Schnelle T, Mueller T (2008) Contact-free single-cell cultivation by negative dielectrophoresis. J Phys D-Appl Phys 41:175502
58. Zhang C, Khoshmanesh K, Mitchell A, Kalantar-zadeh K (2010) Dielectrophoresis for manipulation of micro/nano particles in microfluidic systems. Anal Bioanal Chem 396:401–420
59. Sebastian A, Buckle AM, Markx GH (2007) Tissue engineering with electric fields: immobilization of mammalian cells in multilayer aggregates using dielectrophoresis. Biotechnol Bioeng 98:694–700
60. Ho CT, Lin RZ, Chang WY, Chang HY, Liu CH (2006) Rapid heterogeneous liver-cell on-chip patterning via the enhanced field-induced dielectrophoresis trap. Lab Chip 6:724–734

61. Yue T, Nakajima M, Tajima H, Fukuda T (2013) Fabrication of microstructures embedding controllable particles inside dielectrophoretic microfluidic devices. Int J Adv Robot Syst 10:132
62. Scharnweber T, Truckenmuller R, Schneider AM, Welle A, Reinhardt M, Giselbrecht S (2011) Rapid prototyping of microstructures in polydimethylsiloxane (PDMS) by direct UV-lithography. Lab Chip 11:1368–1371
63. Voldman J, Gray ML, Toner M, Schmidt MA (2002) A microfabrication-based dynamic array cytometer. Anal Chem 74:3984–3990
64. Mittal N, Rosenthal A, Voldman J (2007) NDEP microwells for single-cell patterning in physiological media. Lab Chip 7:1146–1153
65. Yue T, Nakajima M, Takeuchi M, Hu C, Huang Q, Fukuda T (2014) On-chip self-assembly of cell embedded microstructures to vascular-like microtubes. Lab Chip 14:1151–1161
66. Unger MA, Chou HP, Thorsen T, Scherer A, Quake SR (2000) Monolithic microfabricated valves and pumps by multilayer soft lithography. Science 288:113–116
67. Schudel BR, Choi CJ, Cunningham BT, Kenis PJA (2009) Microfluidic chip for combinatorial mixing and screening of assays. Lab Chip 9:1676–1680
68. Mohan R, Schudel BR, Desai AV, Yearsley JD, Apblett CA, Kenis PJ (2011) Design considerations for elastomeric normally closed microfluidic valves. Sensor Actuat B: Chem 160:1216–1223